Journal of Applied Sciences

ISSN 1812-5654

science alert

ANSInet
an open access publisher
http://ansinet.com

Journal of Applied Sciences 13 (14): 2760-2766, 2013
ISSN 1812-5654 / DOI: 10.3923/jas.2013.2760.2766

Speed Identification of Bearingless Induction Motor Based on Least Squares Support Vector Machine Inverse

[1]Zebin Yang, [1]Mingtao Wang, [2]Xiaodong Sun and [1]Huangqiu Zhu
[1]Department of Electrical and Information Engineering,
[2]Automotive Engineering Research Institute, Jiangsu University, 212013, Zhenjiang, China

Abstract: In order to achieve the online detection problem of rotor speed for Bearingless Induction Motor (BIM), a speed identification scheme based on the Least Square Support Vector Machine (LSSVM) inverse is presented in this study. According to the inherent relationship among the variables of BIM, the speed subsystem is first built and proved to be invertible. Secondly, the inverse model was constructed using LSSVM which has good function approximation characteristics. And then the obtained inverse model is combined with this subsystem, which well realized the real-time rotation speed identification. Finally, a vector control simulation platform of BIM is established to evaluate the proposed method. The simulation results demonstrates the proposed LSSVM inverse method can accurately identify the speed parameter in a full speed operation region with good dynamic and static performance.

Key words: Bearingless induction motor (BIM), speed identification, least squares support vector machine (LSSVM), inverse vector control

INTRODUCTION

Bearingless induction motor (BIM), combining the functions of suspension and drive, is a new type of magnetic levitation motor (Bartholet *et al*., 2011; Rodriguez and Santisteban, 2011; Sun and Zhu, 2010). BIM has many good characteristics of traditional induction motor, such as simple structure, low cogging torque, easy weakening control, high reliability. Besides that, it also contains many virtues such as no lubrication, no contact, no noise and long life etc. This makes it has broad application prospects including turbines molecular pump, compressor, high speed electric spindle, aerospace and fly wheel energy storage etc. Now it has been becoming a hot spot of research in the field of special driver/transmission (Chiba *et al*., 2005; Chiba and Asama, 2012; Schuhmann *et al*., 2012; Fang *et al*., 2012).

Currently, the main BIM control strategy is focused on the vector control method which applies magnetic field orientation to achieve high-performance closed-loop speed regulation. However, this control strategy requires a real-time and accurate speed parameter (Chiba and Santisteban, 2012). A traditional method to solve this problem is to install mechanical position or speed sensor, but the installed sensor will increase the system cost and rotational inertia and finally affect the system static and dynamic performance. At the same time, the sensor's performance is easily affected by the material, environment and other factors which degrade the reliability of the control system. Therefore, speed-sensorless operation with online speed identification becomes the technical bottleneck for the BIM to go to the engineering and practical fields. At present, some scholars have carried out many studies on the speed identification for traditional induction motor and have achieved a certain results, but few has studied on the BIM speed identification. Particularly, the operational aspects of BIM with non-speed sensor have not been reported.

In AC drive system, the speed identification principle is based on the motor's non-speed information (such as voltage, current and other physical quantum) with appropriate algorithms. This information can estimate speed information that can replace the mechanical speed sensor (Wang *et al*., 2012). Thus, how to exactly get the motor speed information to meet the requirements of real-time control is the key difficulty of the AC drive system with speed identification. The current speed identification methods mainly have: (1) Estimating speed by detecting the induced electromotive force. This method has good speed identification performance only at high speed, while the speed identification will be ineffective at low or zero speed

Corresponding Author: Zebin Yang, Department of Electrical and Information Engineering, Jiangsu University, 212013, Zhenjiang, China

(Chen *et al*., 2003), (2) Model reference adaptive system (MARS) method. This method based on stability theory has some advantages such as less computation, excellent speed estimation, etc. However, the precise extent of the reference model parameters has a direct impact on the speed identification accuracy (Schauder, 1992; Gadoue *et al*., 2010; Cirrincione and Pucci, 2005), (3) The Kalman filter estimation method. This method uses the minimum variance optimal predictive estimation to weaken the measurement noise and random interference. It is the most common estimation method in the research and application fields, but parameter configuration of this algorithm is lack of a certain standard and the computation is large (Shi *et al*., 2002; Salvatore *et al*., 2010) and (4) High-frequency injection method. This method does not require the coordinate transformation and is not affected by the error of rotor parameter estimation and then it can give satisfied speed estimation even in low and zero speed. However, this method needs to increase the external device to perform the high-frequency signal injection. The expenditure is high and the motor dynamic performance is susceptible to the influence of the injected signal (Kim and Seok, 2011).

BIM is a nonlinear, multivariable, strong coupling system and the mathematical model is very complex. For the existence of parameter change and load disturbance, it is necessary to study the speed identification strategy independent of the parameters and model changes. In recent years, scholars have came up with left inverse system method to realize the effective identification for the parameters that is not direct measured (Huang *et al*., 2010). In this study, the BIM speed left inverse identification strategy based on the LSSVM is proposed that has good nonlinear function approximation characteristics (Zhang *et al*., 2010). This strategy does not totally rely on the BIM system mathematical model and can effectively curb the system external disturbance. The simulated result demonstrates the effectiveness and feasibility of the presented method.

MATHEMATICAL MODEL AND REVERSIBILITY ANALYSIS OF BIM

Ignoring the motor magnetic saturation and iron loss and without regarding to the nonlinear characteristics and time delay of the inverter, in the torque windings rotor flux linkage oriented d-q rotating coordinate system, based on magnetic equivalent circuit method and the virtual displacement theorem, a mathematical model of the BIM can be created:

$$\begin{cases} \dot{i}_{s1d} = \dfrac{L_{m1}}{\sigma L_{s1} L_{r1} T_r}\psi_{r1d} - \dfrac{\left(R_{s1}L_{r1}^2 + R_{r1}L_{m1}^2\right)}{\sigma L_{s1}L_{r1}^2} i_{s1d} + \omega_1 i_{s1q} + \dfrac{u_{s1d}}{\sigma L_{s1}} \\ \dot{i}_{s1q} = -\dfrac{L_{m1}}{\sigma L_{s1} L_{r1}}\omega_r\psi_{r1d} - \dfrac{\left(R_{s1}L_{r1}^2 + R_{r1}L_{m1}^2\right)}{\sigma L_{s1}L_{r1}^2} i_{s1q} - \omega_1 i_{s1d} + \dfrac{u_{s1q}}{\sigma L_{s1}} \\ \dot{\psi}_{r1d} = -\dfrac{1}{T_r}\psi_{r1d} + \dfrac{L_m}{T_r} i_{s1d} \\ \dot{\omega}_r = \dfrac{p_1^2 L_{m1}}{JL_{r1}}\psi_{r1d} i_{s1q} - \dfrac{p_1}{J} T_L \end{cases} \quad (1)$$

where i_{s1d} and i_{s1q} are stator current of torque windings d-axis and q-axis, respectively; u_{s1d} and u_{s1q} are stator voltage of torque windings d-axis and q-axis, respectively; $\varnothing_{r1d}$ is d-axis rotor flux linkage of torque windings; $R_{r1}$and R_{s1} are the rotor and stator resistance of torque windings, respectively; L_{r1}, L_{s1} and L_{m1} are the rotor and stator self-inductance and mutual inductance of torque windings, respectively; p_1 is the pole-pair number of torque windings; ω_r and ω_1 are the angular velocity and synchronous angular velocity of rotor, respectively; J is rotation inertia; $T_r = L_{r1}/R_{r1}$, $\sigma = 1 - L_{m1}^2/\left(L_{s1}L_{r1}\right)$.

State variables are chosen as:

$$\boldsymbol{x} = [x_1, x_2, x_3, x_4]^T = [i_{s1d}, i_{s1q}, \psi_{r1d}, \omega_r]^T$$

Input variables are chosen as:

$$\boldsymbol{y} = [y_1, y_2]^T = [x_3, x_4]^T = [\psi_{r1d}, \omega_r]^T$$

Control variables are chosen as:

$$\boldsymbol{u} = [u_1, u_2]^T = [u_{s1d}, u_{s1q}]^T$$

From the analysis of this dynamic system model, it can be seen that the d-axis stator current x_1 and q-axis stator current x_2 can be directly measure. If Eq. 1 can be written in another form, that is, the equation with x_4 as the input and the measurable state variables as output is of the system and this model satisfies the left inverse conditions, then its left inverse is a dynamic model with x_4 as output and measurable variable and their derivatives as input. Putting this left inverse system in series with the original system, we can obtain a equivalent composite system which realize the online measurement of test variable x_4. The principle is shown in Fig. 1.

So, we select the first two equations in Eq. 1 to constitute the mathematical model of the subsystem:

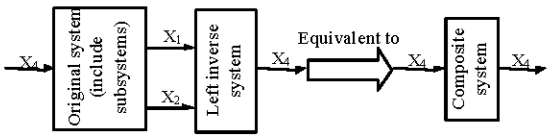

Fig. 1: Speed identification scheme based on left inverse

$$\begin{cases} \dot{x}_1 = \dfrac{L_{m1}}{\sigma L_{s1}L_{r1}T_r}x_3 - \dfrac{\left(R_{s1}L_{r1}^2 + R_{r1}L_{m1}^2\right)}{\sigma L_{s1}L_{r1}^2}x_1 + \omega_1 x_2 + \dfrac{u_1}{\sigma L_{s1}} \\ \dot{x}_2 = -\dfrac{L_{m1}}{\sigma L_{s1}L_{r1}}x_3x_4 - \dfrac{\left(R_{s1}L_{r1}^2 + R_{r1}L_{m1}^2\right)}{\sigma L_{s1}L_{r1}^2}x_2 - \omega_1 x_1 + \dfrac{u_2}{\sigma L_{s1}} \end{cases} \quad (2)$$

Then, we choose measurable variables x_1, x_2 and their derivatives to constitute speed subsystem and verify its reversibility.

According to Eq. 2, the Jacobi matrix can be constituted as:

$$A(x,u) = \begin{bmatrix} \dfrac{\partial \dot{x}_1}{\partial x_3} & \dfrac{\partial \dot{x}_1}{\partial x_4} \\ \dfrac{\partial \dot{x}_2}{\partial x_3} & \dfrac{\partial \dot{x}_2}{\partial x_4} \end{bmatrix} = \begin{bmatrix} \dfrac{L_{m1}}{\sigma L_{s1}L_{r1}T_r} & 0 \\ -\dfrac{L_{m1}x_4}{\sigma L_{s1}L_{r1}T_r} & -\dfrac{L_{m1}x_3}{\sigma L_{s1}L_{r1}T_r} \end{bmatrix} \quad (3)$$

Then:

$$\mathrm{Det}(A(x,u)) = -\frac{L_{m1}^2}{\sigma^2 L_{s1}^2 L_{r1}^2 T_r}x_3 \quad (4)$$

It follows from Eq. 4 that $\mathrm{Det}(A(x,u)) \neq 0$ and then the matrix A(x,u) is nonsingular when $x_3 \neq 0$. According to the inverse function theorem, the speed subsystem (2) is reversible and its inverse can be expressed as:

$$x_4 = f(x_1, x_2, \dot{x}_1, \dot{x}_2, u_{s1d}, u_{s1q}, i_{s1d}, i_{s1q}, \omega_1) \quad (5)$$

where, f(.) is a complex nonlinear function whose analytical expression is difficult to obtain. We can use the nonlinear function approximation ability of LSSVM to establish the inverse model.

SPEED IDENTIFICATION OF BIM BASED ON LSSVM INVERSE

The objective of LSSVM is to determine the optimal function $y(x) = \omega^T\varphi(x) + b$ to regress an unknown function, where $\omega_i \in R^m$ and $b \in R$ are the weight vector and bias value, respectively, $\varphi(x)$ is the nonlinear mapping from input space to feature space. Using this mapping, n groups of training samples (x_i, y_i) in the original space are mapped to high-dimensional feature space. LSSVM training can be done by solving the following optimization problem:

$$\begin{cases} \min J(\omega,\varepsilon) = \dfrac{1}{2}\omega^T\omega + \dfrac{\gamma}{2}\sum_{i=1}^{n}\varepsilon_i^2 \\ \text{s.t.} \quad y_i = \omega^T\varphi(x_i) + b + \varepsilon_i, i = 1,2,\cdots n \end{cases} \quad (6)$$

where, ϵ_i is the relaxation factor of insensitive loss function, γ is the regularization parameter.

The optimization problem (6) can be transformed to an optimization problem by introducing the Lagrangian multipliers a_i, that is, the following Lagrangian function:

$$L(\omega,a,b,\varepsilon) = J(\omega,\varepsilon) - \sum_{i=1}^{n} a_i\left(y_i - \omega^T\varphi(x_i) - b - \varepsilon_i\right) \quad (7)$$

where

$$\omega = (\varepsilon_1, \varepsilon_2, \cdots \varepsilon_n)^T,\ a = (a_1, a_2, \cdots a_n)^T$$

From KKT conditions, this optimization problem can be transformed into solving the following linear equations by calculating the partial derivative of Langrangian function (7):

$$\begin{bmatrix} 0 & 1 & \cdots & 1 \\ 1 & K(x_1,x_1) + \dfrac{1}{\gamma} & \cdots & K(x_1,x_n) \\ \vdots & \vdots & \ddots & \vdots \\ 1 & K(x_n,x_1) & \cdots & K(x_n,x_n) + \dfrac{1}{\gamma} \end{bmatrix} \begin{bmatrix} b \\ a_1 \\ \vdots \\ a_n \end{bmatrix} = \begin{bmatrix} 0 \\ y_1 \\ \vdots \\ y_n \end{bmatrix} \quad (8)$$

where $K(x_i,y_j)$ is a kernel function satisfying the Mercer condition. We choose the RBF kernel function as:

$$K(x_i,x_j) = \exp\left(\frac{-\left|x_i - x_j\right|^2}{2\sigma^2}\right) \quad (9)$$

where σ is the kernel width. The values of a and b can be obtained from Eq. 8 and then ω can be obtained from Eq. 7. Finally, we can get the L SSVM function regression expressed as:

$$y(x) = \sum_{i=1}^{n} a_i K(x_i,x) + b \quad (10)$$

Based on the above analysis, the LSSVM inverse model of BIM speed can be established (Fig. 2). where the model input is the two-phase voltage u_{s1d}, u_{s1q},

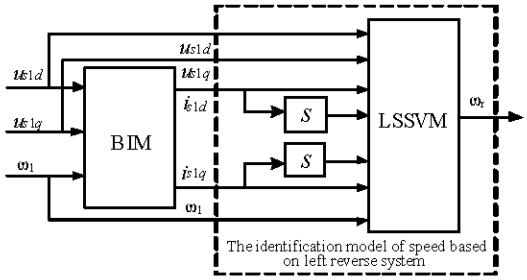

Fig. 2: Speed observation schematic illustration of BIM based on left inverse system.

two-phase current i_{s1d}, i_{s1q}, as well as motor synchronous angular velocity ω_1 and two phase current differential.

CONTROL SYSTEM STRUCTURE OF SPEED IDENTIFICATION FOR BIM BASED ON LSSVM INVERSE

BIM control system is composed of the electromagnetic torque and radial suspension force control. The electromagnetic torque control is based on the rotor field orientation vector control of torque windings. While, the radial suspension force control is relatively complex. First, we detect rotor radial displacement using the displacement sensor and then calculate the reference radial suspension forces. Secondly, using the force/current transformation, suspension force windings current signals are achieved to carry out the precise control of the radial displacement. BIM radial suspension force in the d-q.

Rotating coordinate system is as follows:

$$\begin{cases} F_x = K(i_{s2d}\Psi_{1d} + i_{s2q}\Psi_{1q}) \\ F_y = K(i_{s2q}\Psi_{1d} - i_{s2d}\Psi_{1q}) \end{cases} \quad (11)$$

where, in the d-q rotating coordinate system, F_x and F_y are radial suspension force, respectively. i_{s2d} and i_{s2q} are the stator current components of suspension force windings, respectively. $\varnothing_{1d}$ and $\varnothing_{1q}$ are the air-gap flux linkage of torque windings, respectively. $K=K_m+K_l$:

$$K_m = \frac{\pi p_1 p_2 L_{m2}}{18\mu_0 l r W_1 W_2}$$

$$K_l = \frac{p_1 W_2}{2rW_1}$$

L_{m2} is suspension force windings mutual inductance, p_2 is the pole-pair number of the suspension force windings, W_1 and W_2 are the number of turns of torque windings and suspension force windings per phase in series, respectively. μ_0 is the vacuum permeability, r is the BIM stator inner diameter, l is BIM stator core length.

We have $\varnothing_{r1d} = \varnothing_{r1}$, $\varnothing_{r1q} = 0$ when the torque windings rotor field oriented control strategy is applied. The following equation can be obtained:

$$\begin{cases} i_{s1d} = \dfrac{T_r p + 1}{L_{m1}}\Psi_{r1} \\ i_{s1q} = \dfrac{T_e L_{r1}}{p_1 L_{m1}\Psi_{r1}} \\ \omega_s = \dfrac{L_{m1}}{T_{r1}\Psi_{r1}} i_{s1q} \\ T_e = p_1 \dfrac{L_{m1}}{L_{r1}} i_{s1q}\Psi_{r1} \end{cases} \quad (12)$$

where, ω_s is the rotary slip. According to the relationship between the torque windings air-gap flux linkage and rotor flux linkage, air-gap flux linkage component can be got by the following equation:

$$\begin{cases} \Psi_{1d} = \dfrac{L_{m1}}{L_{r1}}(\Psi_{r1d} + L_{r1l} i_{s1d}) \\ \Psi_{1q} = \dfrac{L_{m1}}{L_{r1}} L_{r1l} i_{s1q} \end{cases} \quad (13)$$

where, L_{r1l} is rotor leakage inductance of torque windings. Based on the air-gap flux linkage values of torque windings, the current value of the suspension force windings can be determined through the Eq. 11:

$$\begin{bmatrix} i_{s2d} \\ i_{s2q} \end{bmatrix} = \frac{1}{M}\begin{bmatrix} \cos\rho & -\sin\rho \\ \sin\rho & \cos\rho \end{bmatrix}\begin{bmatrix} F_x \\ F_y \end{bmatrix} \quad (14)$$

Where:

$$M = K\sqrt{\Psi_{1d}^2 + \Psi_{1q}^2},\ \rho = \arctan(\Psi_{1q}/\Psi_{1d})$$

Figure 3 shows the diagram of the BIM control system based on LSSVM inverse speed identification. With rotor field oriented control strategy, the air-gap flux linkage of torque windings can be observed by Eq. 13 and the rotor radial displacement can be obtained by the position sensors.

SIMULATION ANALYSIS

In order to validate the feasibility and effectiveness of the proposed speed identification, we carry a simulation with an experimental prototype. BI parameters as follows: the power is 1kW, The suspension force windings (pole-pair number is p_2 = 1) and the torque

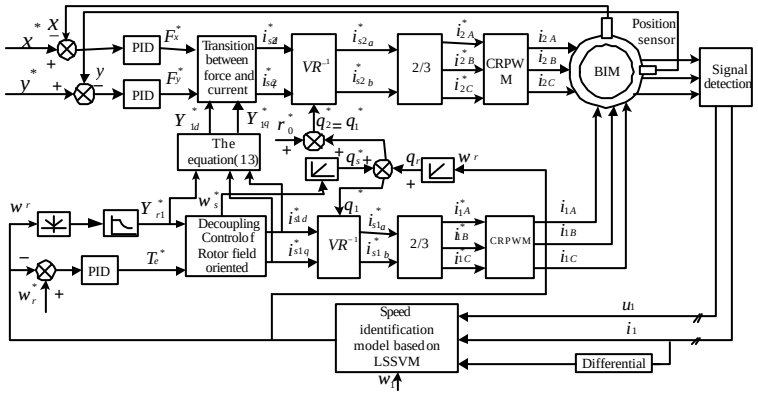

Fig. 3: Control system structure of speed identification for BIM

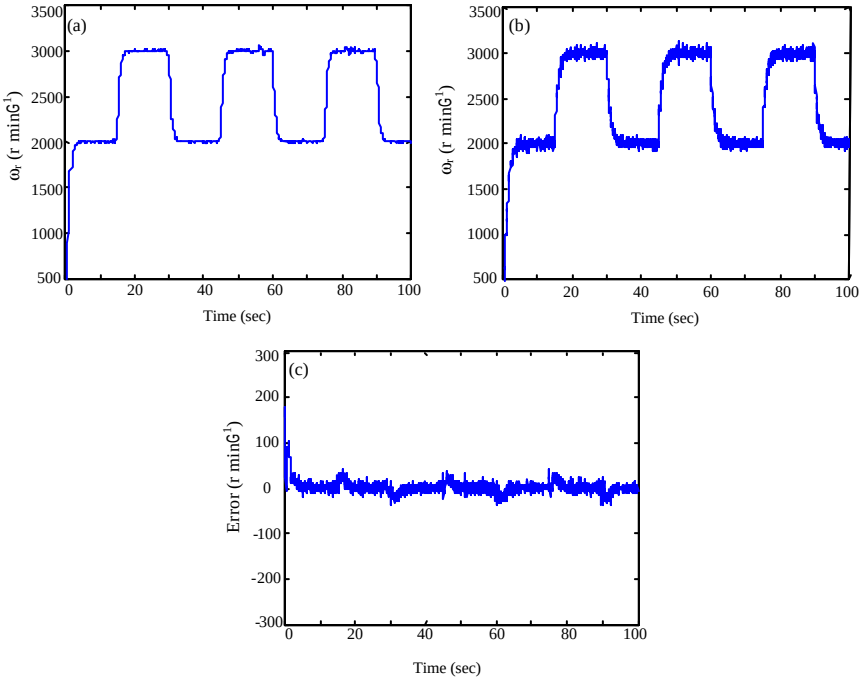

Fig. 4(a-c): Simulation results of tracking rectangle-wave (a) Actual output of speed, (b) Identification output of speed and (c) Error

windings (pole-pair resistance is 11.48 Ω, rotor inductance is 16.778×10^{-2} H, the mutual inductance between the stator and rotor is 15.856×10^{-2} H, rotor time constant is 1.46×10^{-2} sec, the rotary inertia is 0.00769 kg•m^2, the rotor mass is 2.85 kg.

In the actual operating range of BIM, we sample u_{s1d}, u_{s1q}, i_{s1d}, i_{s1q} real time as input, ω as output, then we calculate the first derivative of the two-phase current i_{s1d}, i_{s1q} using high-precision seven-point numerical algorithm. In this way, the training sample set $\{u_{s1d}, u_{s1q}, i_{s1d}, i_{s1d}, i_{s1q}, i_{s1q}\}$ and $\{\omega_r\}$ can be constituted. Note that the sample set of data has a difference magnitude on the quantity. In order to overcome the disadvantage of the slow convergence when LSSVM is trained, the training sample set of data is normalized.

LSSVM recognition accuracy largely depends on the selection of core width σ and the regularization parameter γ. In order to improve the modeling accuracy of the BIM's speed left inverse model, we use cross-validation method to determine the core width σ and regularization parameters γ which makes LSSVM possess good generalization capability and then improve the speed recognition effects. By crossover procedure, the resulting parameters for σ = 1400, γ = 2.6.

Figure 4 shows a simulation waveform of system trajectory with rectangular wave reference input. The

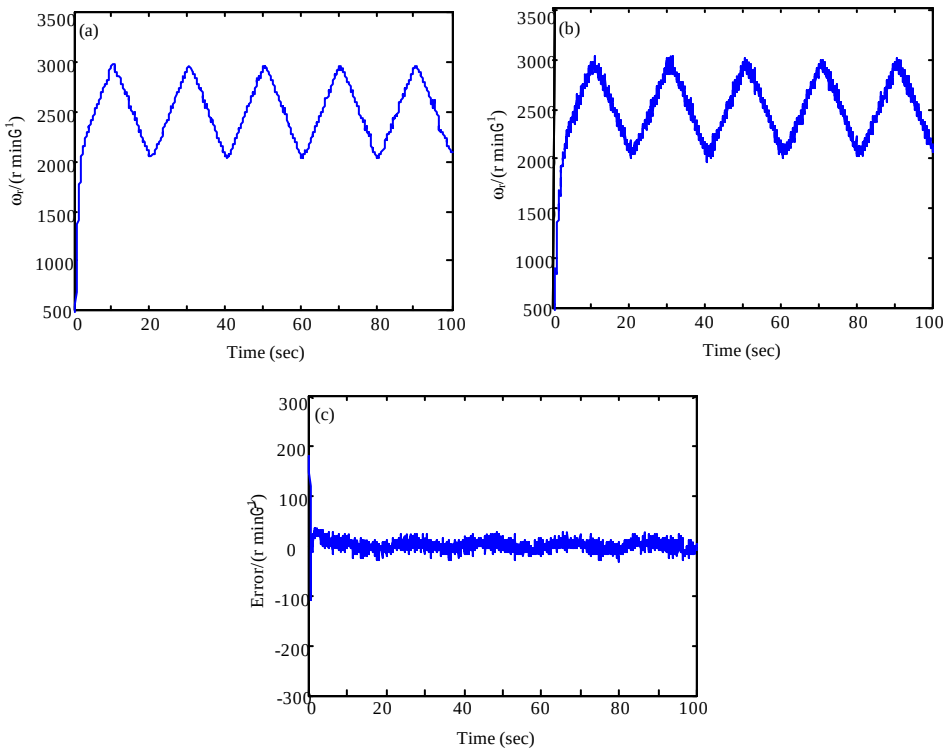

Fig. 5(a-c): Simulation results of tracking triangle-wave (a) Actual output of speed, (b) Identification output of speed and (c) Error

amplitude of this rectangular wave changes from 2000 r min^{-1} to 3000 r min^{-1}. Figure 4a shows the actual speed waveform and Fig. 4b shows the identified speed based on LS-SVM inverse and Fig. 4c shows the error between the actual speed and identified one. Figure 5 shows a simulation waveform of system trajectory the triangular wave reference input. The amplitude of triangular wave changes from 2000 to 3000 r min^{-1}. Figure 5a shows the actual speed. Figure 5b shows the identified speed based on LS-SVM inverse and Fig. 5c shows the error between the actual speed and identified one.

It can be seen from Fig. 4 and 5 that the identified speed can track the rectangular wave and triangular wave when the LSSVM inverse identification strategy is applied. This system has good dynamic performance and high identification precision. The maximum error between actual speed and identified speed is lower than 20 r min^{-1}.

CONCLUSION

In this study, a BIM's speed identification strategy is presented by using the LSSVM inverse. The proposed strategy can overcome the limitation of the physical speed sensor built in the BIM. In order to achieve this target, the existence of the left inverse model of speed subsystem is proved. And then the LSSVM left inverse mode is constructed using the structure of the LSSVM and differentiator. The proposed speed identification strategy is independent of the mathematical model and parameter change. As demonstrated in the result, the accuracy, static and dynamic performance can be ensured by using the method. Furthermore, the presented method gives a new way for the study of speed-sensorless operation.

ACKNOWLEDGEMENT

This study was supported by the National Natural Science Foundation of China (61104016, 51305170); Science Foundation of Jiangsu Province of China (BK20130515); China Post Doctoral Science Foundation Funded Project (2012M521012); Natural Project Funded by the Priority Academic Program Development of Jiangsu Higher Education Institutions (201106).

REFERENCES

Bartholet, M.T., T. Nussbaumer and J.W. Kolar, 2011. Comparison of voltage-source inverter topologies for two-phase bearingless slice motors. IEEE Trans. Ind. Electr., 58: 1921-1925.

Chen, Z., M. Tomita, S. Doki and S. Okuma, 2003. An extended electromotive force model for sensorless control of interior permanent-magnet synchronous motors. IEEE Trans. Ind. Electr., 50: 288-295.

Chiba, A., T. Fukao, O. Ichikawa, M. Oshima, M. Takemoto and D.G. Dorrell, 2005. Magnetic Bearings and Bearingless Drives. Elsevier Newnes Press, Boston, MA., ISBN: 9780080478975, Pages: 400.

Chiba, A. and J. Asama, 2012. Influence of rotor skew in induction type bearingless motor. IEEE Trans. Magnet., 48: 4646-4649.

Chiba, A. and J.A. Santisteban, 2012. A PWM harmonics elimination method in simultaneous estimation of magnetic field and displacements in bearingless induction motors. IEEE Trans. Ind. Appli., 48: 124-131.

Cirrincione, M. and M. Pucci, 2005. Sensorless direct torque control of an induction motor by a TLS-based MRAS observer with adaptive integration. Automatica, 41: 1843-1854.

Fang, J., S. Zheng and B. Han, 2012. Attitude sensing and dynamic decoupling based on active magnetic bearing of MSDGCMG. IEEE Trans. Instrumentation Measurement, 61: 338-348.

Gadoue, S.M., D. Giaouris and J.W. Finch, 2010. MRAS sensorless vector control of an induction motor using new sliding-mode and fuzzy logic adaptation mechanisms. IEEE Trans. Energy Conversion, 25: 394-402.

Huang, Y.H., Y.K. Sun, B. Wang, X.G. Zhu and C.G. Xia, 2010. Research of soft sensor based on fuzzy neural network inverse system for lysine fermentation process. Chin. J. Scientific Instrument, 31: 862-865.

Kim, S.K. and J.K. Seok, 2011. High-frequency signal injection-based rotor bar fault detection of inverter-fed induction motors with closed rotor slots. IEEE Trans. Ind. Appli., 47: 1624-1631.

Rodriguez, E.F. and J.A. Santisteban, 2011. An improved control system for a split winding bearingless induction motor. IEEE Trans. Ind. Electr., 58: 3401-3408.

Salvatore, N., A. Caponio, F. Neri, S. Stasi and G.L. Cascella, 2010. Optimization of delayed-state kalman-filter-based algorithm via differential evolution for sensorless control of induction motors. IEEE Trans. Ind. Electr., 57: 385-394.

Schauder, C., 1992. Adaptive speed identification for vector control of induction motors without rotational transducers. IEEE Trans. Ind. Appl., 28: 1054-1061.

Schuhmann, T., W. Hofmann and R. Werner, 2012. Improving operational performance of active magnetic bearings using Kalman filter and state feedback control. IEEE Trans. Ind. Electr., 59: 821-829.

Shi, K.L., T.F. Chan, Y.K. Wong and S.L. Ho, 2002. Speed estimation of an induction motor drive using an optimized extended Kalman filter. Ind. Electronics IEEE Trans., 49: 124-133.

Sun, X.D. and H.Q. Zhu, 2010. Decoupling control of bearingless induction motors based on neural network inverse system method. Trans. China Electrotechnical Soc., 25: 43-49.

Wang, L.P., H.G. Zhang and X.C. Liu, 2012. Integral backstepping controller in the sensorless vector-control system for permanent magnet synchronous motor. Control Theory Appli., 29: 199-204.

Zhang, S.N., F.N. Wang, D.K. He and J. Runda, 2010. Soft sensing prcobalt oxalate particle size based on multiple LS-SVM regssion. Chin. J. Scientific Instrument, 31: 2081-2087.